eLIFE
elifesciences.org

Figures and figure supplements

The 133-kDa N-terminal domain enables myosin 15 to maintain mechanotransducing stereocilia and is essential for hearing

Qing Fang, et al.

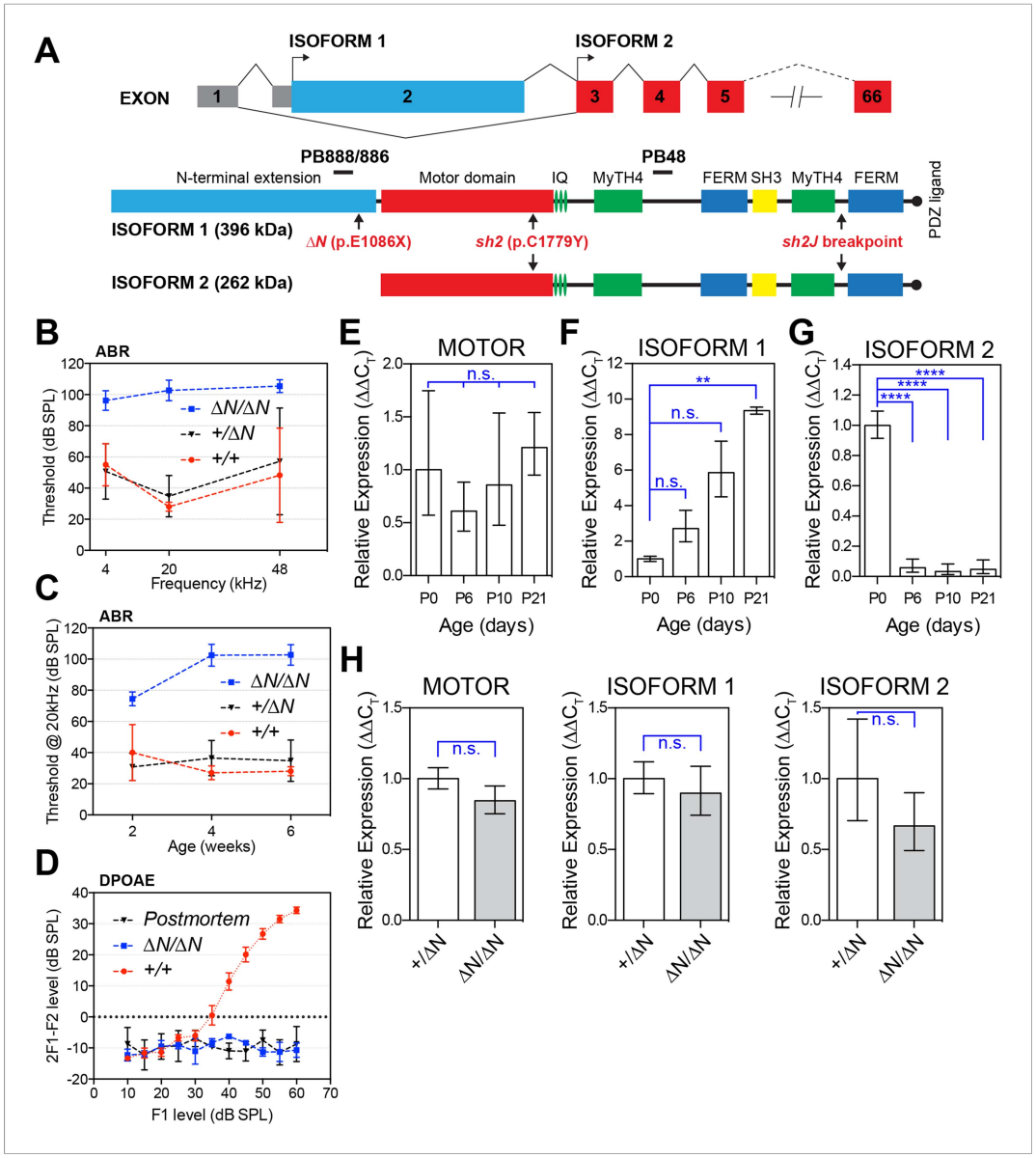

Figure 1. A mutation targeting isoform 1 causes deafness in *Myo15*$^{\Delta N/\Delta N}$ mice. (**A**) Two protein isoforms are generated from alternatively spliced transcripts of *Myo15*. Transcripts incorporating exon 2 encode isoform 1 (396 kDa; Genbank: NM_010862.2), while exclusion of this exon produces isoform 2 (262 kDa; Genbank: NM_182698.2). Both isoforms have identical motor and tail domains, including a PDZ ligand, SH3, MyTH4 and FERM moieties. The mutant *Myo15* alleles used in this study are shown along with antibody epitopes. (**B**) Auditory brainstem response (ABR) thresholds at 4, 20 and 48 kHz for *Myo15*$^{+/+}$, *Myo15*$^{+/\Delta N}$ and *Myo15*$^{\Delta N/\Delta N}$ mice at 6 weeks of age. Data are mean ± SD (n = 3–6 animals per group). (**C**) ABR thresholds at 20 kHz, measured from 2, 4 and 6 weeks old *Myo15*$^{+/+}$, *Myo15*$^{+/\Delta N}$ and *Myo15*$^{\Delta N/\Delta N}$ mice. Data are mean ± SD (n = 3–6 animals per group). (**D**) Distortion product otoacoustic emission (DPOAE) levels (2F1-F2) at 12 kHz in *Myo15*$^{+/+}$ and *Myo15*$^{\Delta N/\Delta N}$ mice at 6 weeks. Data are mean ± SD (n = 3–4 animals per group). (**E**–**G**) Relative expression of *Myo15* isoforms in wild-type cochleae measured with RT-qPCR at ages indicated. Probes target exon junction 13–14, detecting the motor domain common to both isoforms 1 and 2 (**E**); exon junction 2–3, detecting isoform 1 (**F**); exon junction 1–3, detecting isoform 2 (**G**). Relative expression $2^{-}(-\Delta\Delta C_T)$ for each *Myo15* transcript was normalized first to the housekeeping gene (*Tbp*) and then to the respective isoform expression at P0. The total expression of both isoforms remains stable (**E**), however there is a transition from isoform 2 to isoform 1, which becomes the dominant mRNA species by P21 (see ***Figure 1—figure supplement 1D***). Data are mean ± SD (n = 3–5 biological replicates per condition). Asterisks indicate significance: n.s., $p > 0.05$; **, $p < 0.01$; ****, $p < 0.0001$ (ANOVA with Tukey's multiple comparison test). (**H**) Identical qPCR probes were used to assay *Myo15* expression in *Myo15*$^{+/\Delta N}$ and *Myo15*$^{\Delta N/\Delta N}$ cochleae at P0. Relative expression $2^{-}(-\Delta\Delta C_T)$ values were normalized to *Tbp* and then to expression in

Figure 1. continued on next page

Figure 1. Continued

heterozygous *Myo15*$^{+/\Delta N}$ samples. Data are mean ± SD (n = 3–4 biological replicates per condition). n.s., $p > 0.05$ (*t*-test of independent variables).

DOI: 10.7554/eLife.08627.003

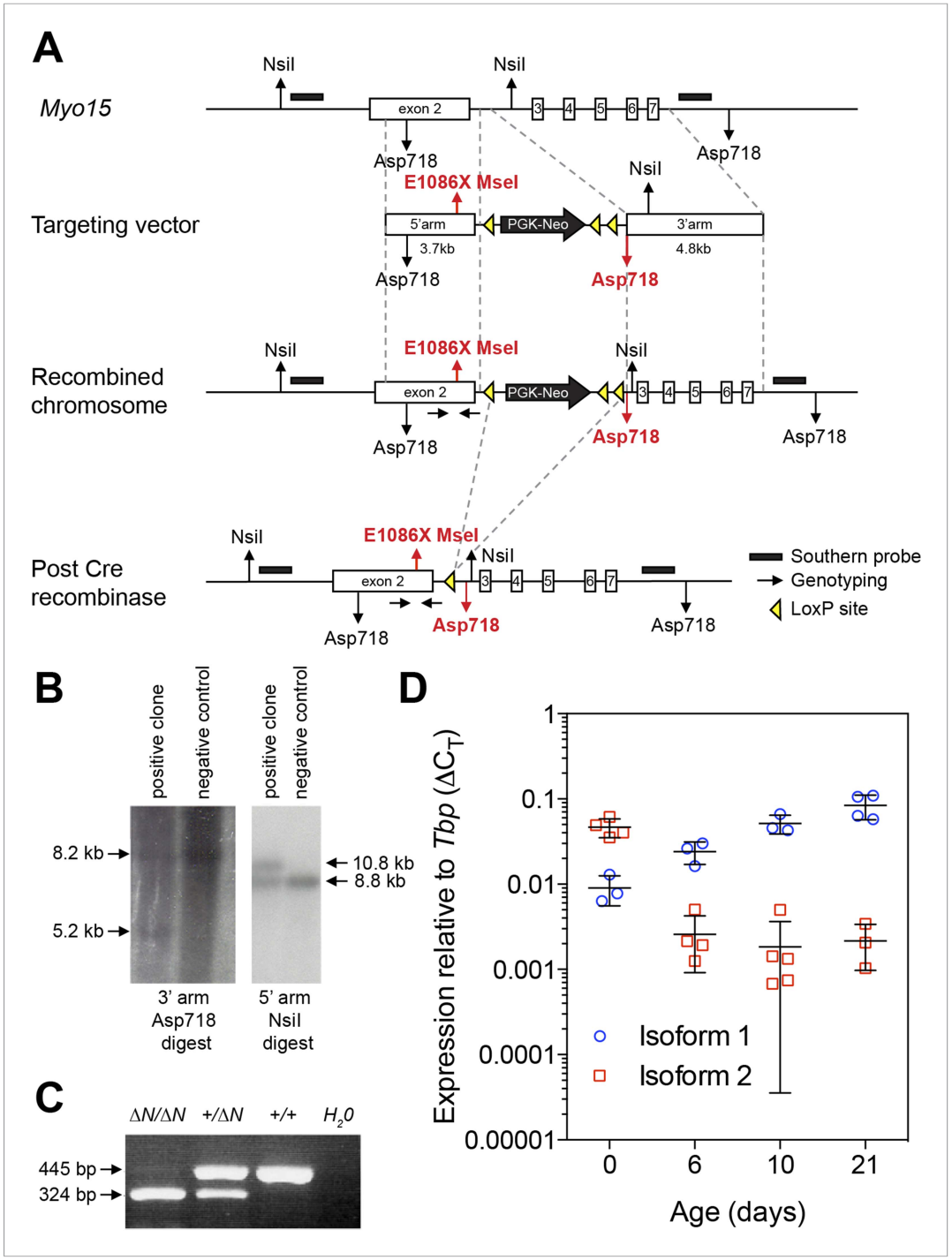

Figure 1—figure supplement 1. Generation of a mouse model for human p.E1105X DFNB3 deafness. (**A**) Genomic locus of the wild-type mouse *Myo15* allele and targeting strategy to introduce the p.E1086X mutation into exon 2 by homologous recombination. Southern blot probes (black bars) and *loxP* sites (yellow triangles) are shown. A single *loxP* site remains after excision of the PGK-Neo cassette by *cre* recombinase. Restriction sites unique to the recombined allele are highlighted in red. Homozygous mutants of both sexes were fertile and obtained in normal Mendelian ratios expected for an autosomal recessive allele (data not shown). (**B**) Validation of homologous recombination by Southern blot analysis. ES cell genomic DNA was digested with *Asp718* (left panel) or *NsiI* (right panel) and hybridized with DNA probes to the 3′ arm (left panel) or 5′ arm (right panel). The restriction fragment sizes expected for a correctly recombined locus are shown (arrows). (**C**) PCR confirmation of germ-line transmission

Figure 1—figure supplement 1. continued on next page

Figure 1—figure supplement 1. Continued

from mouse tail genomic DNA. Introduction of the p.E1086X mutation creates a new *MseI* endonuclease restriction site that is used for genotyping. Amplicons were digested with *MseI* and restriction fragments analyzed by gel electrophoresis. The expected restriction fragments for different genotypes are shown (arrows). (**D**) Quantitative PCR (qPCR) analysis of *Myo15* isoform expression in mouse cochleae. The qPCR data for isoforms 1 and 2 (previously presented in ***Figure 1***), were reanalyzed as fold changes ($2^{-}\Delta C_T$) relative to the housekeeping gene *Tbp*. Note: the large errors bars at day 10 are due to the use of semi-logarithmic axes.

DOI: 10.7554/eLife.08627.004

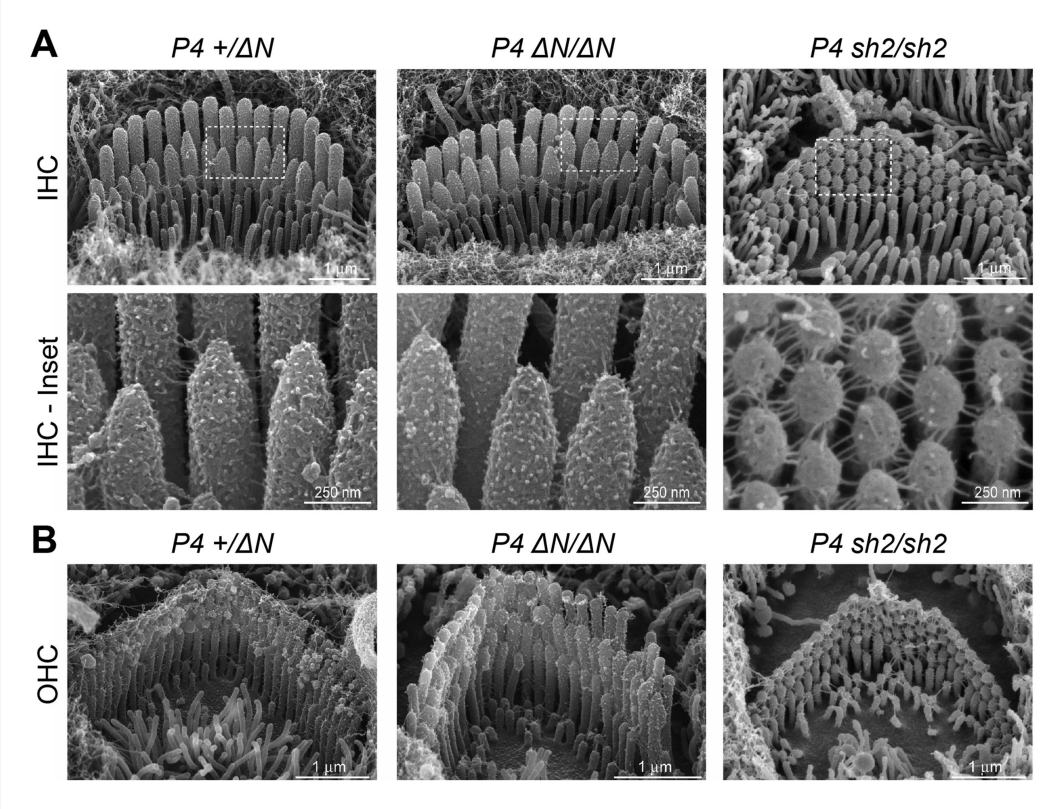

Figure 2. *Myo15*$^{\Delta N/\Delta N}$ hair cells initially develop normal stereocilia bundles. (**A**, **B**) Scanning electron microscopy (SEM) of inner (**A**) and outer (**B**) hair cells from *Myo15*$^{\Delta N/\Delta N}$, normal hearing *Myo15*$^{+/\Delta N}$ littermates and *Myo15*$^{sh2/sh2}$ cochleae at P4. Highlighted regions of IHC bundles (white boxes) are shown at higher magnification below. *Myo15*$^{\Delta N/\Delta N}$ stereocilia bundles develop the characteristic staircase architecture (see ***Figure 7—figure supplement 2***) that is strikingly absent from age-matched *Myo15*$^{sh2/sh2}$ hair cells. Scale bars are 1 µm (**A**, upper row and **B**) and 250 nm (**A**, lower row).

DOI: 10.7554/eLife.08627.005

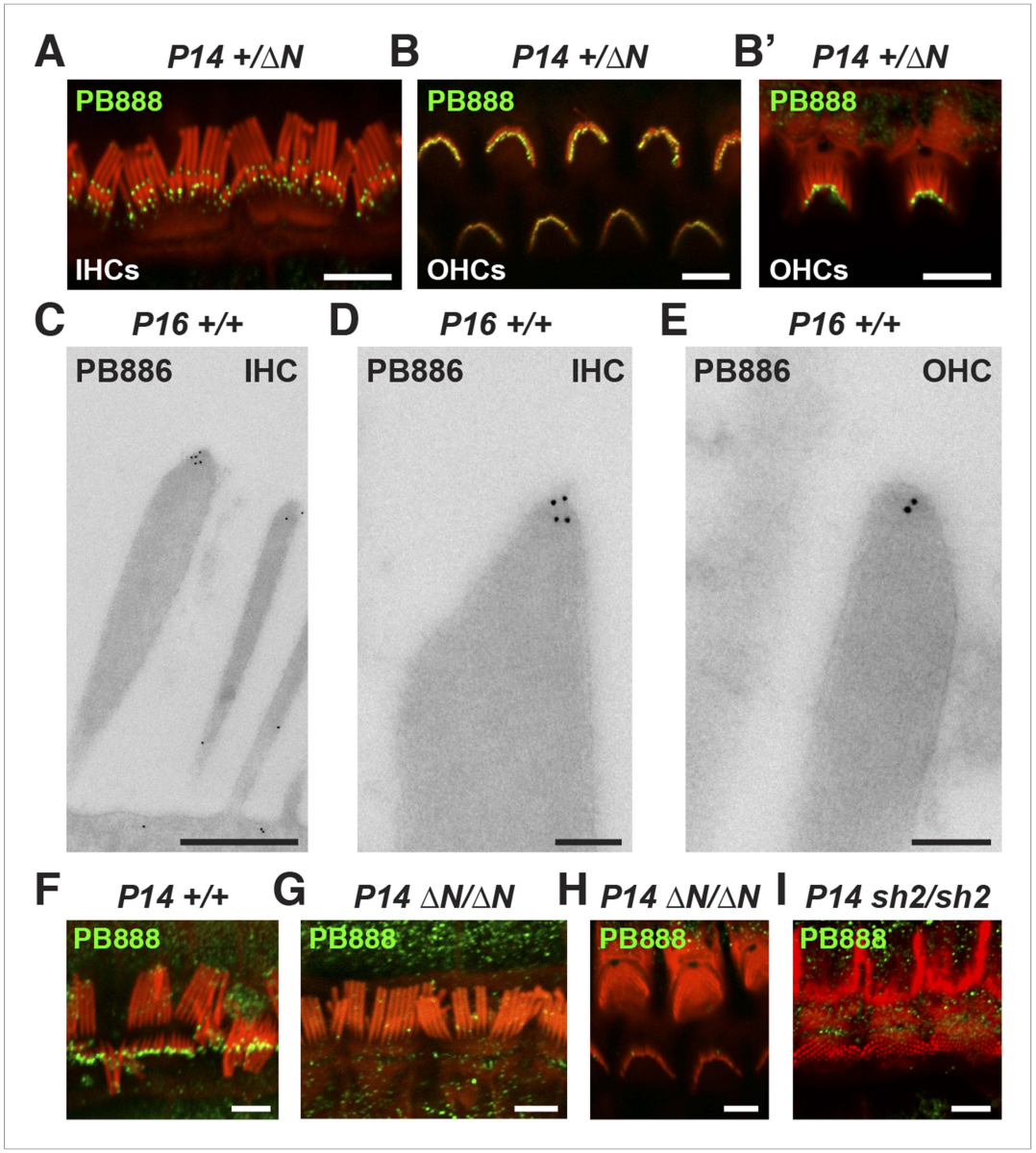

Figure 3. Isoform 1 targets to the tips of shorter mechanotransducing stereocilia. (**A**) PB888 antibody (green) detects isoform 1 at the tips of shorter row stereocilia of IHCs from normal hearing *Myo15*$^{+/\Delta N}$ mice. (**B**) Isoform 1 is present at the tips of all stereocilia in OHCs of normal hearing *Myo15*$^{+/\Delta N}$ mice at P14. An oblique view confirms the presence of isoform 1 on the tallest row (**B′**). (**C**–**E**) TEM micrographs of immuno-gold labeled PB886 in ultrathin stereocilia sections. Isoform 1 is localized in proximity to the stereocilia tip density. Labeling was infrequently observed along the stereocilia core. (**F**) PB888 does not localize to the upper tip-link insertion point on the tallest IHC stereocilia row in intentionally splayed bundles. (**G**, **H**) Loss of reactivity in *Myo15*$^{\Delta N/\Delta N}$ IHCs and OHCs confirms the loss of isoform 1 protein from the hair bundle and the specificity of PB888 labeling. (**I**) PB888 does not label the stereocilia tips in *Myo15*$^{sh2/sh2}$ hair cells which have the p.C1779Y motor domain mutation. Scale bars are 5 μm (**A**, **B**, **B′**, **F**, **G**–**I**), 500 nm (**C**), 100 nm (**D**, **E**). Immunofluorescence samples are counter-stained with rhodamine phalloidin (red) to reveal the stereocilia actin cytoskeleton. See also ***Figure 3—figure supplement 1***.

DOI: 10.7554/eLife.08627.008

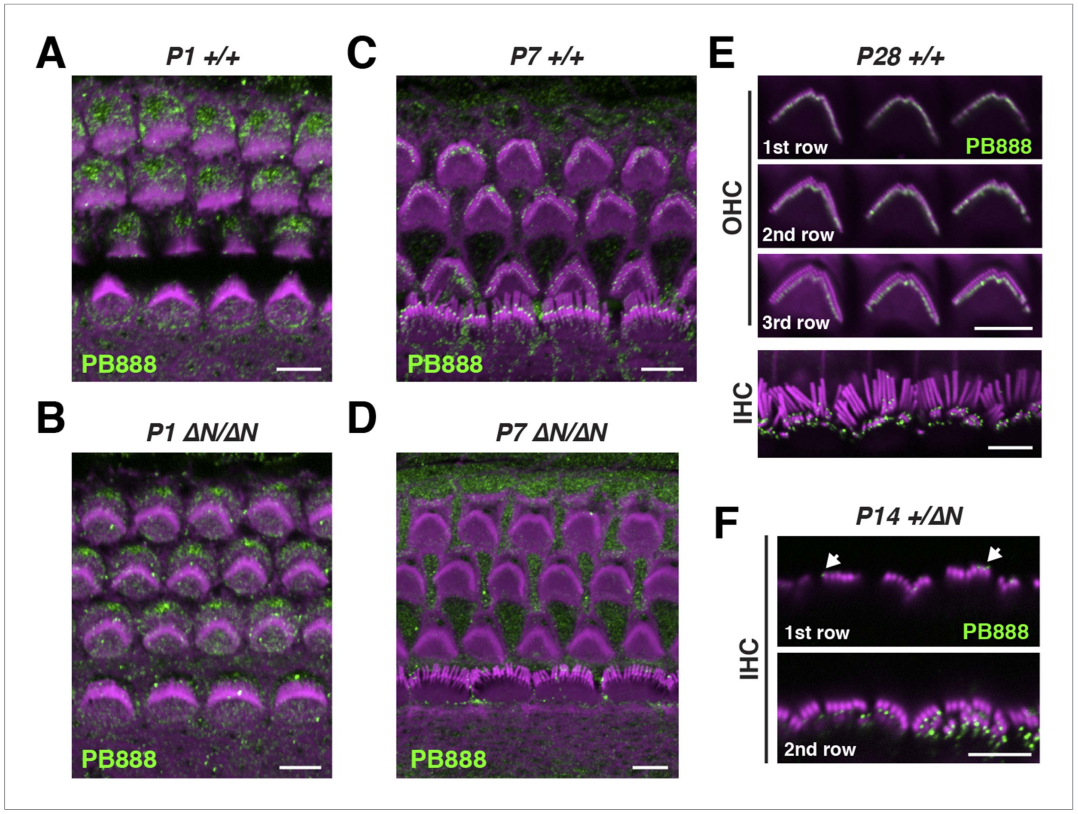

Figure 3—figure supplement 1. Isoform 1 localization during cochlear development. (**A**–**D**) PB888 antibody labeling (green) of isoform 1 in cochlear whole mounts from wild-type *Myo15*$^{+/+}$ (**A**, **C**) and isoform 1-null *Myo15*$^{\Delta N/\Delta N}$ (**B**, **D**) cochleae at P1 (**A**, **B**) and P7 (**C**, **D**). (**E**) PB888 antibody (green) in adult wild-type *Myo15*$^{+/+}$ IHCs and OHCs at P28. The same OHCs are presented at different focal planes to show the tips of each stereocilia row. (**F**) PB888 antibody (green) in normal *Myo15*$^{+/\Delta N}$ IHCs at P14. Two focal planes of the same IHCs are shown. Note the presence of isolated punctae (arrows) on the tallest row. Rhodamine phalloidin (magenta) labels actin filaments in all panels. Scale bars are 5 μm.

DOI: 10.7554/eLife.08627.009

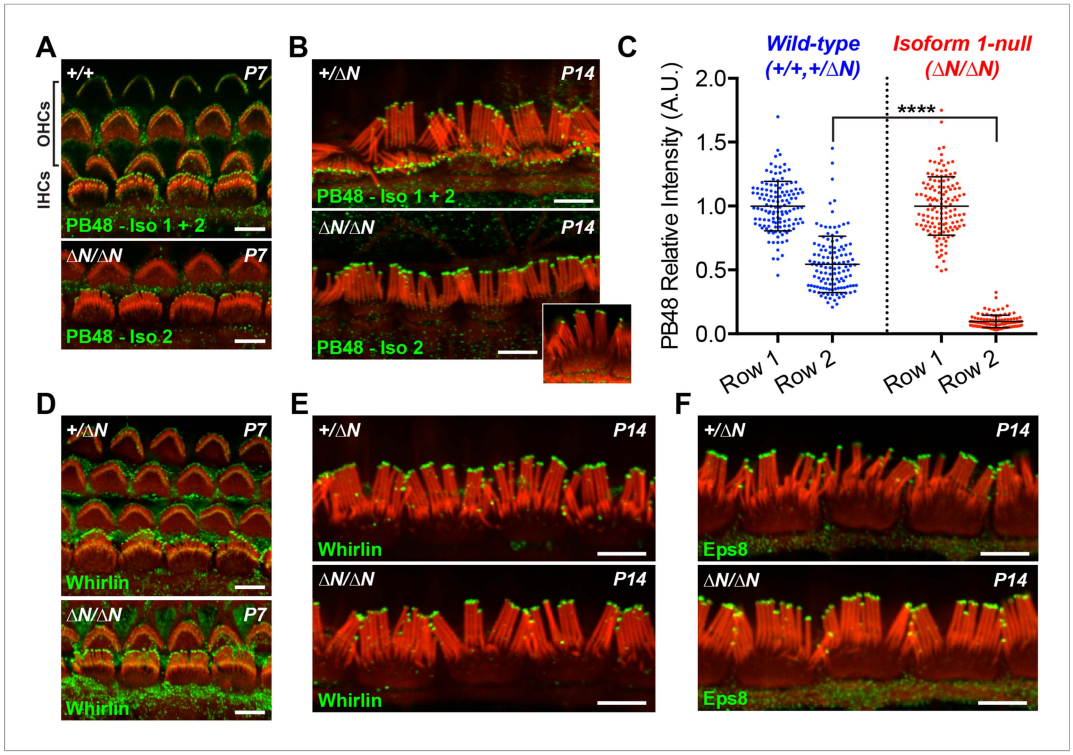

Figure 4. Isoform 2 traffics predominantly to the tallest stereocilia row and is sufficient to target Eps8 and Whirlin. (**A**, **B**) PB48 antibody (green) was raised to an epitope common to isoforms 1 and 2 (***Figure 1A***) and labels all stereocilia rows in wild-type *Myo15*$^{+/+}$ and *Myo15*$^{+/\Delta N}$ hair cells at P7 (**A**) and P14 (**B**). In isoform 1-null *Myo15*$^{\Delta N/\Delta N}$ hair cells, PB48 is predominantly detected on the tallest stereocilia row at P7 (**A**) and at P14 (**B**), identifying isoform 2 at these locations. (**C**) Quantification of PB48 fluorescence on the shorter second stereocilia row of IHCs at P7 normalized to the first (tallest) row. Data points represent individual stereocilia from wild-type (blue, *Myo15*$^{+/+}$ and *Myo15*$^{+/\Delta N}$ combined, n = 125 stereocilia, 3 animals) or *Myo15*$^{\Delta N/\Delta N}$ (red, n = 112 stereocilia, n = 4 animals) IHCs at P7, overlaid with mean ± SD. Asterisks indicate significance: *, $p < 0.0001$ (*t*-test of independent variables). (**D**, **E**) Whirlin antibody localizes primarily to the tallest stereocilia row of control *Myo15*$^{+/\Delta N}$ hair cells at P7 (**D**) and at P14 (**E**). The localization of whirlin remains unchanged in isoform 1-null *Myo15*$^{\Delta N/\Delta N}$ hair cells at P7 (**D**) or P14 (**E**). (**F**) Eps8 antibody localizes primarily to the tallest stereocilia row of control *Myo15*$^{+/\Delta N}$ and isoform 1-null *Myo15*$^{\Delta N/\Delta N}$ IHCs at P14. All samples are co-labeled with rhodamine phalloidin (red). Scale bars are 5 μm.

DOI: 10.7554/eLife.08627.010

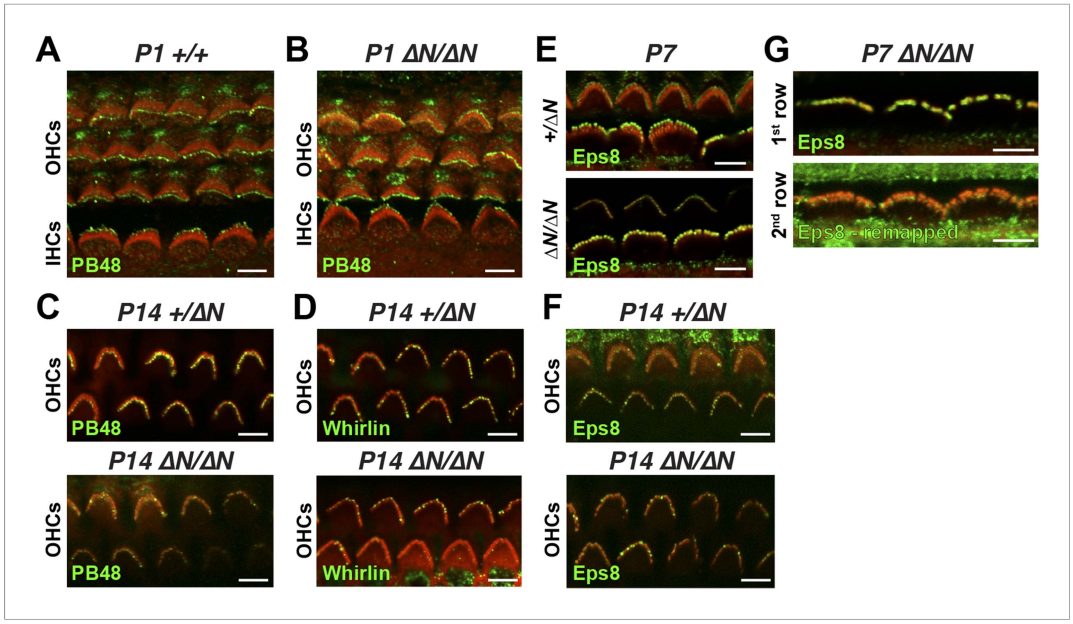

Figure 4—figure supplement 1. Isoform 2 is sufficient to traffic Eps8 and Whirlin within the hair bundle. (**A**, **B**) PB48 labeling (green) of isoforms 1 and 2 in whole mount *Myo15*$^{+/+}$ (**A**) and isoform 1-null *Myo15*$^{\Delta N/\Delta N}$ (**B**) hair cells at P1. (**C**) PB48 labeling (green) of P14 *Myo15*$^{+/\Delta N}$ (top panel) and *Myo15*$^{\Delta N/\Delta N}$ OHCs (lower panel). (**D**) Whirlin antibody (HL5136) labeling (green) of *Myo15*$^{+/\Delta N}$ (top panel) and *Myo15*$^{\Delta N/\Delta N}$ (lower panel F) OHCs at P14. (**E** and **F**) Eps8 antibody labeling (green) in *Myo15*$^{+/\Delta N}$ (upper panels) and *Myo15*$^{\Delta N/\Delta N}$ (lower panels) hair cells at P7 (**E**) and P14 (**F**). Only OHCs are shown at P14 (**F**). (**G**) Alternate view of stereocilia bundles in *Myo15*$^{\Delta N/\Delta N}$ IHCs labeled for Eps8 at P7. The Eps8 antibody signal on the second row was boosted (remapped) to reveal weak labeling at the tips. Actin filaments are labeled in all samples with rhodamine phalloidin (red). Scale bars are 5 μm.

DOI: 10.7554/eLife.08627.011

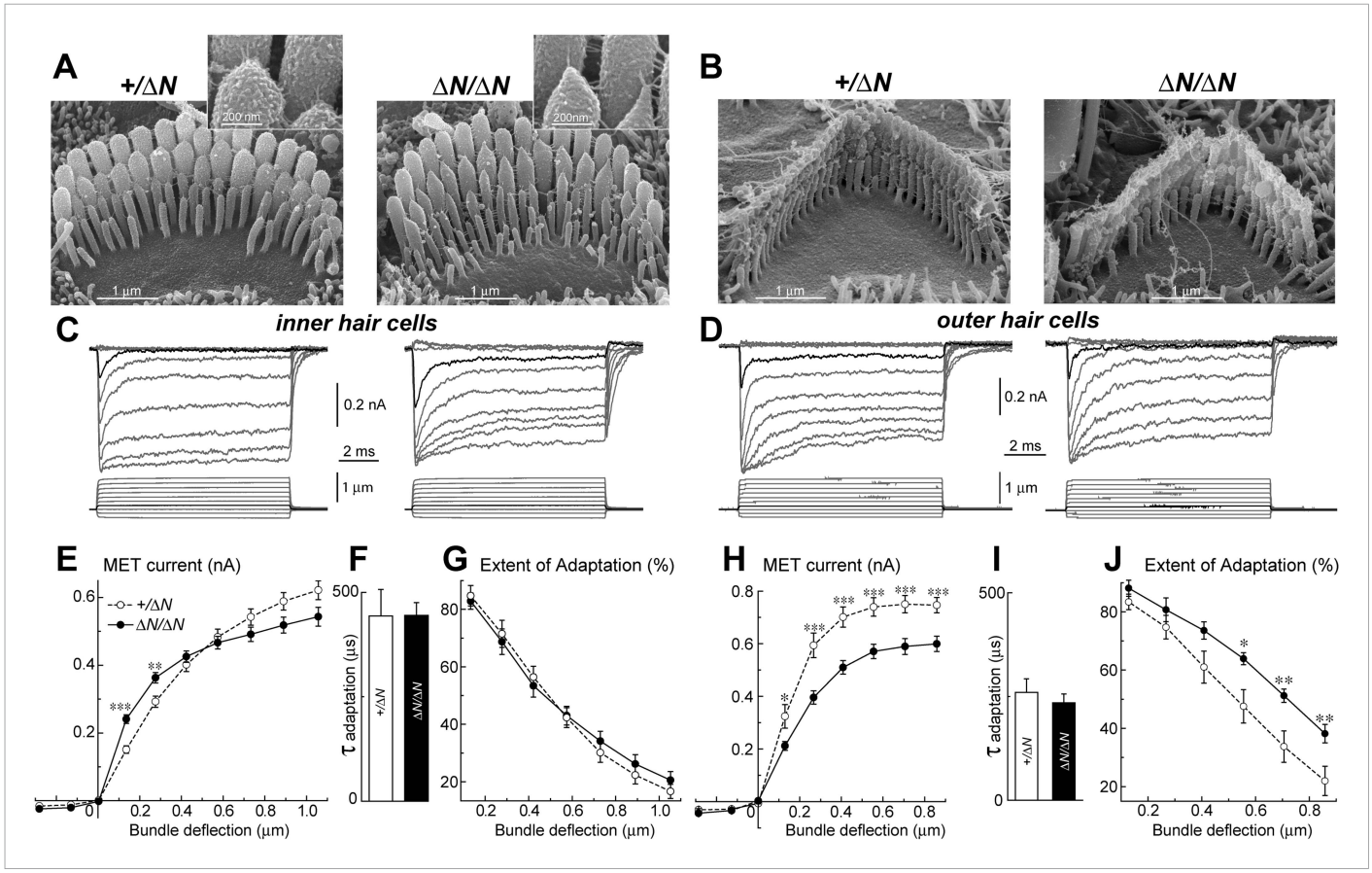

Figure 5. Isoform 1 is not required for MET but influences the deflection sensitivity of IHCs. (**A**, **B**) SEM images of IHC (**A**) and OHC (**B**) stereocilia bundles in *Myo15*$^{+/\Delta N}$ (left panels) and *Myo15*$^{\Delta N/\Delta N}$ (right panels) hair cells. Higher magnification of the second row IHC stereocilia tips are shown (inset). (**C**, **D**) Whole cell current responses (top traces) evoked by graded deflections of the stereocilia bundles (bottom traces) in IHCs (**C**) and OHCs (**D**) in *Myo15*$^{+/\Delta N}$ (left) and *Myo15*$^{\Delta N/\Delta N}$ (right) hair cells. (**E**, **H**) Relationship between the peak MET current and stereocilia bundle displacement in IHCs (**E**) and OHCs (**H**) from *Myo15*$^{+/\Delta N}$ (open circles) and *Myo15*$^{\Delta N/\Delta N}$ (closed circles) cochleae. (**F**, **I**) Time constants of MET adaptation in IHCs (**F**) and OHCs (**I**) for *Myo15*$^{\Delta N/\Delta N}$ and *Myo15*$^{+/\Delta N}$. Time constants were determined from a single exponential fit of MET responses evoked by the small bundle deflections of ~150 nm (see black traces in **C**, **D**). (**G**, **J**) Percent changes of the MET current 10 ms after a stimulation step (extent of adaptation) as a function of stimulus intensity in IHCs (**G**) and OHCs (**J**). The same MET records contribute to all averaged data. Data are mean ± SE. Asterisks indicate statistical significance: *, $p < 0.01$; **, $p < 0.001$; ***, $p < 0.0001$ (*t*-test of independent variables). Holding potential was −90 mV. Age of the cells: P3-4 + 3–5 days in vitro. SEM images were obtained from cultured samples used for MET recordings. Number of cells: n = 10 (IHCs, *Myo15*$^{+/\Delta N}$), n = 12 (IHCs, *Myo15*$^{\Delta N/\Delta N}$), n = 7 (OHCs, *Myo15*$^{+/\Delta N}$), n = 9 (OHCs, *Myo15*$^{\Delta N/\Delta N}$).

DOI: 10.7554/eLife.08627.012

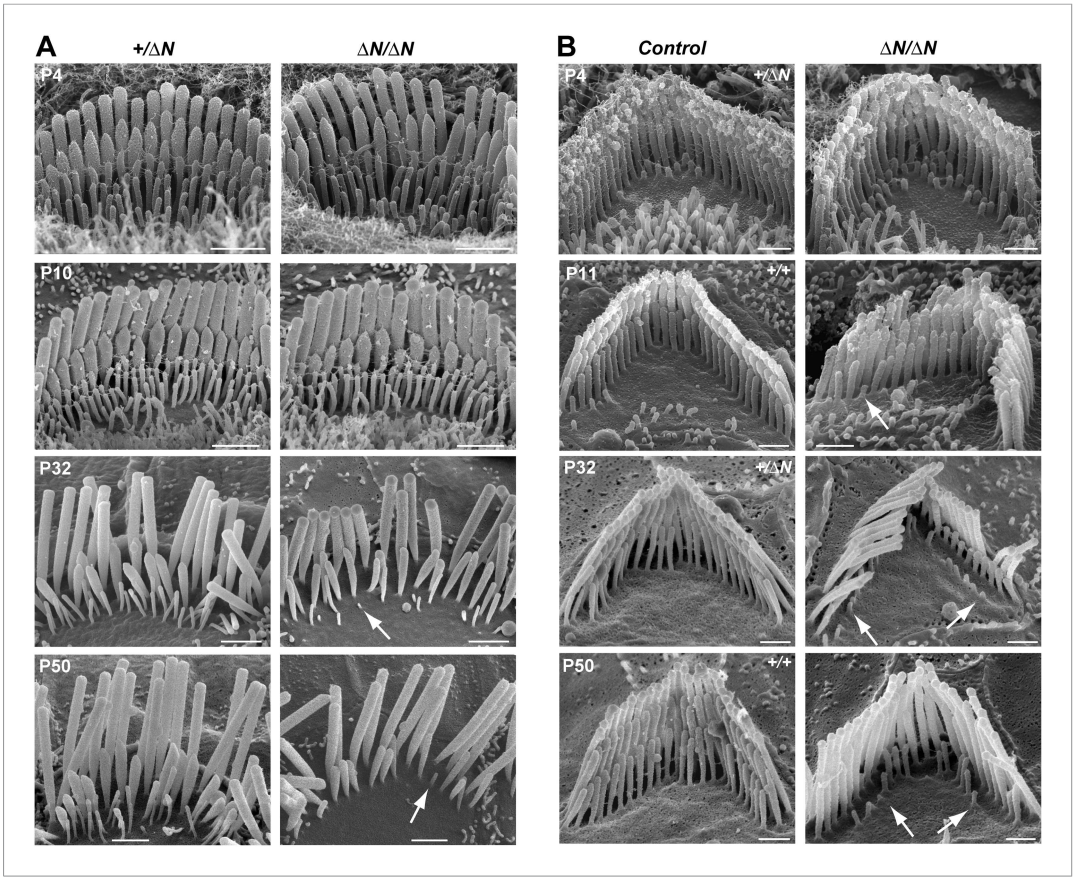

Figure 6. Degeneration of mechanotransducing shorter row stereocilia in isoform 1-null hair cells. (**A**) SEM micrographs of IHC stereocilia bundles of normal *Myo15*$^{+/\Delta N}$ (left) and *Myo15*$^{\Delta N/\Delta N}$ mutant (right) mice at different stages of postnatal development. Arrows point to examples of almost completely resorbed stereocilia. Note that the tallest stereocilia row does not thin, or shorten. (**B**) SEM micrographs of OHC stereocilia bundles show a similar degeneration pattern to IHCs. Shorter row stereocilia are retracted (arrows) but the tallest stereocilia row remains unaffected. All cells were located approximately at the middle of the cochlea. Scale bars are 1 μm (**A**) and 0.5 μm (**B**). See also ***Figure 6—figure supplement 1*** and ***Table 1***.

DOI: 10.7554/eLife.08627.006

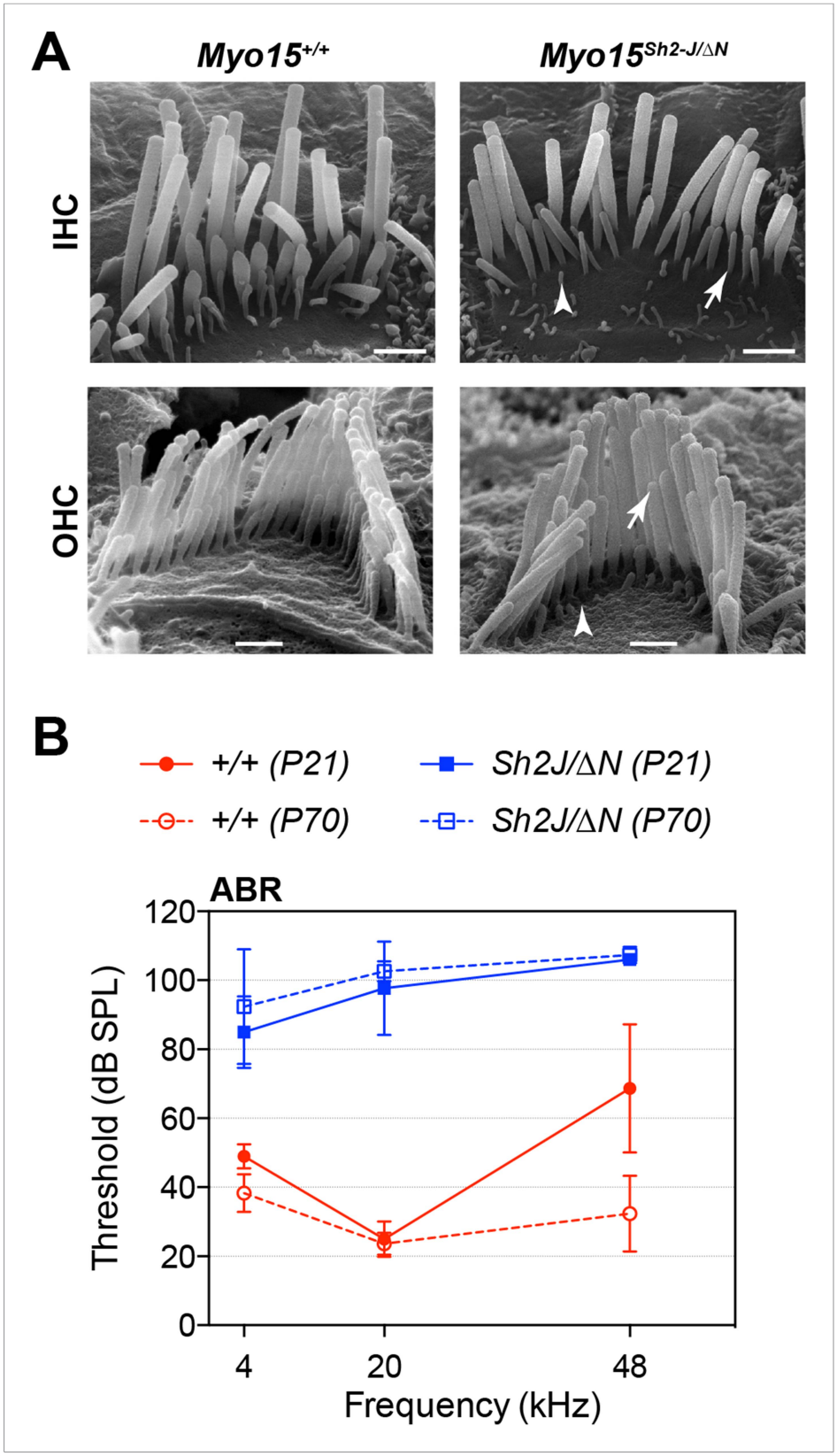

Figure 6—figure supplement 1. *Myo15*$^{sh2\text{-}J}$ does not complement *Myo15*$^{\Delta N}$. (**A**) Scanning electron micrographs of

Figure 6—figure supplement 1. continued on next page

Figure 6—figure supplement 1. Continued

stereocilia hair bundles from wild-type *Myo15*$^{+/+}$ and *Myo15*$^{sh2\text{-}J/\Delta N}$ compound heterozygotes at P28. The shorter stereocilia rows in compound heterozygotes undergo retraction (arrows) and resorption (arrowheads) similar to *Myo15*$^{\Delta N/\Delta N}$ hair cells (see ***Figure 6***). Scale bars are 1 μm (IHCs) and 0.5 μm (OHCs). (**B**) ABR thresholds measured at 4, 20 and 48 kHz in *Myo15*$^{+/+}$ and *Myo15*$^{sh2\text{-}J/\Delta N}$ mice at P21 and P70. Compound heterozygotes have profound hearing impairment at both ages tested.

DOI: 10.7554/eLife.08627.007

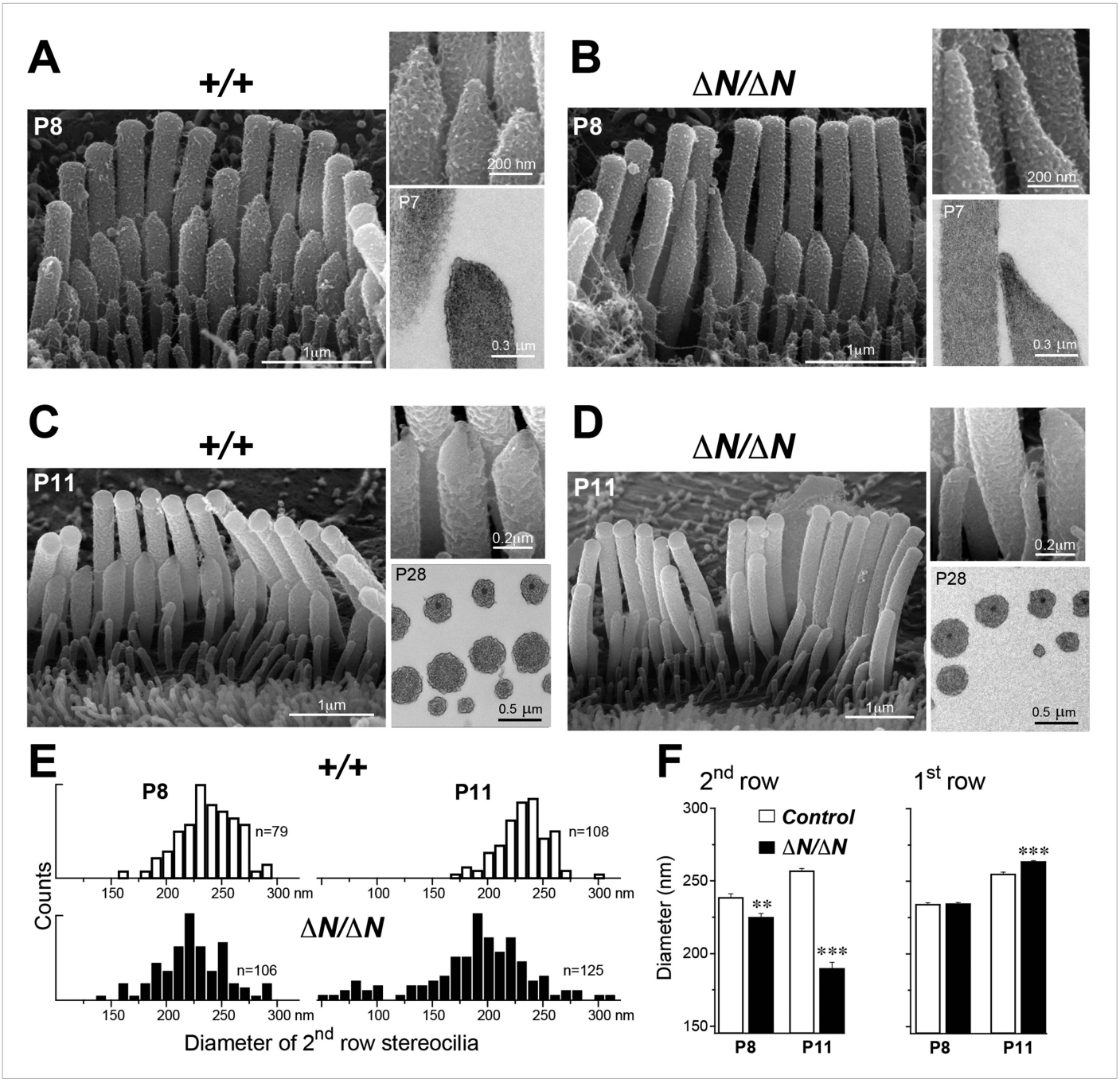

Figure 7. Isoform 1 maintains the diameter of mature mechanosensitive stereocilia and regulates the actin cytoskeleton at their tips. (**A**–**D**) SEM images of stereocilia bundles from *Myo15*$^{+/+}$ and *Myo15*$^{\Delta N/\Delta N}$ IHCs at P8 (**A**, **B**) and P11 (**C**, **D**). The inset (top right) is a higher magnification image of the second row stereocilia tips. The insets (lower right) are TEM images of either longitudinal (**A**, **B**) or axial (**C**, **D**) cross-sections of the stereocilia core. Note the electron-dense material at the tips of *Myo15*$^{\Delta N/\Delta N}$ stereocilia (**B**) and similar density of actin filaments in the thinning stereocilia of second row *Myo15*$^{\Delta N/\Delta N}$ IHCs (**D**). (**E**) Distribution of diameters of second row stereocilia in *Myo15*$^{+/+}$ (upper histogram) and *Myo15*$^{\Delta N/\Delta N}$ (lower histogram) IHCs at P8 (left), and at P11 (right). The diameters were measured from SEM images and are likely underestimated by ~30% due to the uniform tissue shrinkage during critical point drying. Number of IHCs: n = 9 (P8, *Myo15*$^{+/\Delta N}$), n = 9 (P8, *Myo15*$^{\Delta N/\Delta N}$), n = 8 (P11, *Myo15*$^{+/\Delta N}$), n = 8 (P11, *Myo15*$^{\Delta N/\Delta N}$). (**F**) Average diameter of stereocilia in the first and second rows of *Myo15*$^{+/+}$ (white bars) and *Myo15*$^{\Delta N/\Delta N}$ (black bars) IHC bundles at P8 and P11 (data from panel E). Data are shown as mean ± SE. Asterisks indicate statistical significance: **, $p < 0.001$; ***, $p < 0.0001$ (*t*-test of independent variables).

DOI: 10.7554/eLife.08627.014

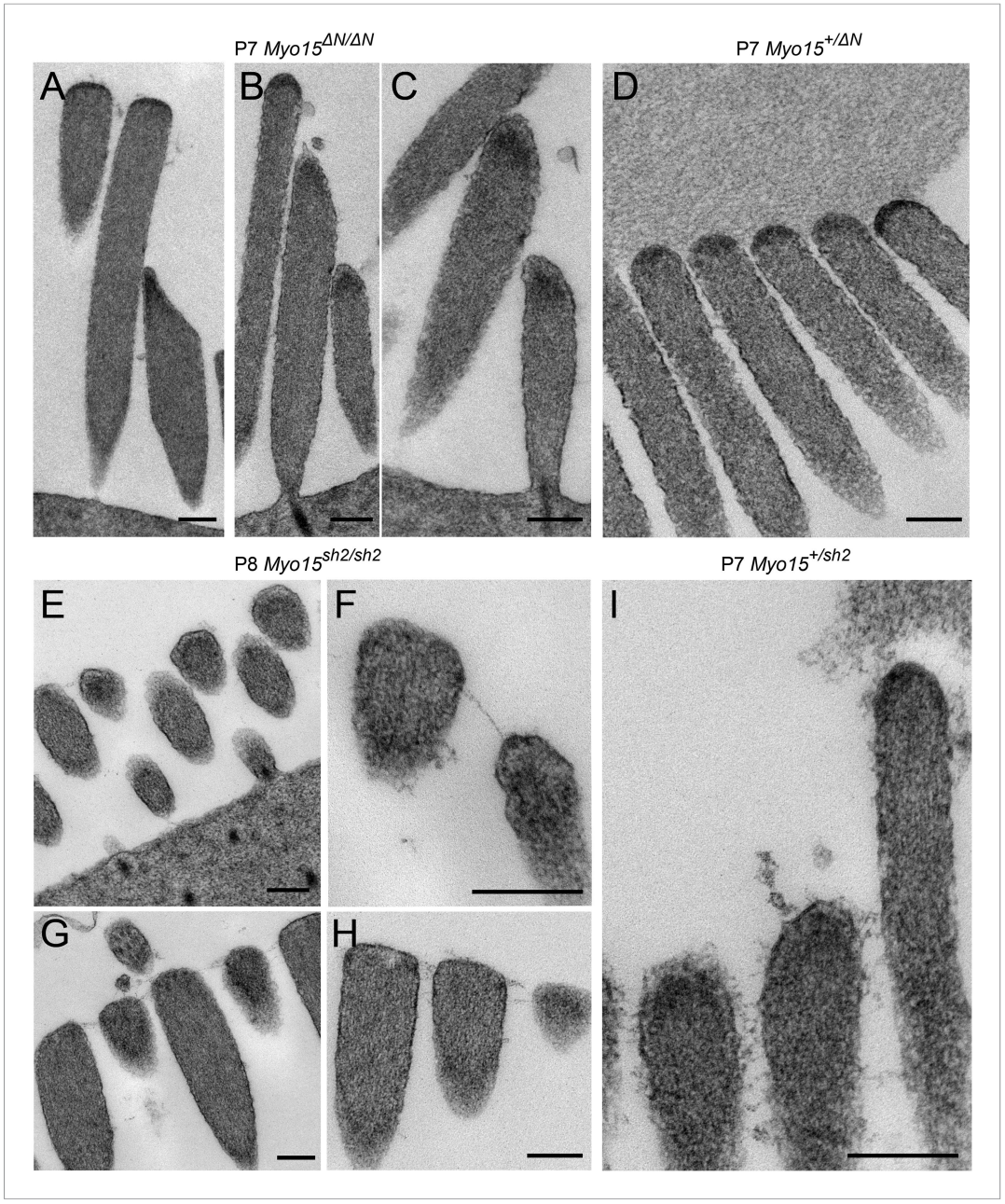

Figure 7—figure supplement 1. Isoform 2 is necessary for tip density formation. (**A**–**D**) TEM images of IHCs (**A**) and OHCs (**B**–**D**) stereocilia bundles in P7 *Myo15*$^{\Delta N/\Delta N}$ and control *Myo15*$^{+/\Delta N}$ littermates. An electron-dense material (arrows) is present at the tips of stereocilia of all rows in both isoform 1-null *Myo15*$^{\Delta N/\Delta N}$ (**A**–**C**) and *Myo15*$^{+/\Delta N}$ (**D**) littermates. (**E**–**I**) TEM images of OHCs (**E**, **F**, **I**) and IHCs (**G**, **H**) stereocilia bundles in P8 *Myo15*$^{sh2/sh2}$ and P7 *Myo15*$^{+/sh2}$ mice. The electron-dense material at the tips of stereocilia is absent from *Myo15*$^{sh2/sh2}$ stereocilia that lack isoforms 1 and 2 (arrows), compared with *Myo15*$^{+/sh2}$. Note: the smaller insertional tip density (arrowheads) can be still observed in P8 *Myo15*$^{sh2/sh2}$ hair cells (**F**, **H**). Scale bars are 200 nm.

DOI: 10.7554/eLife.08627.015

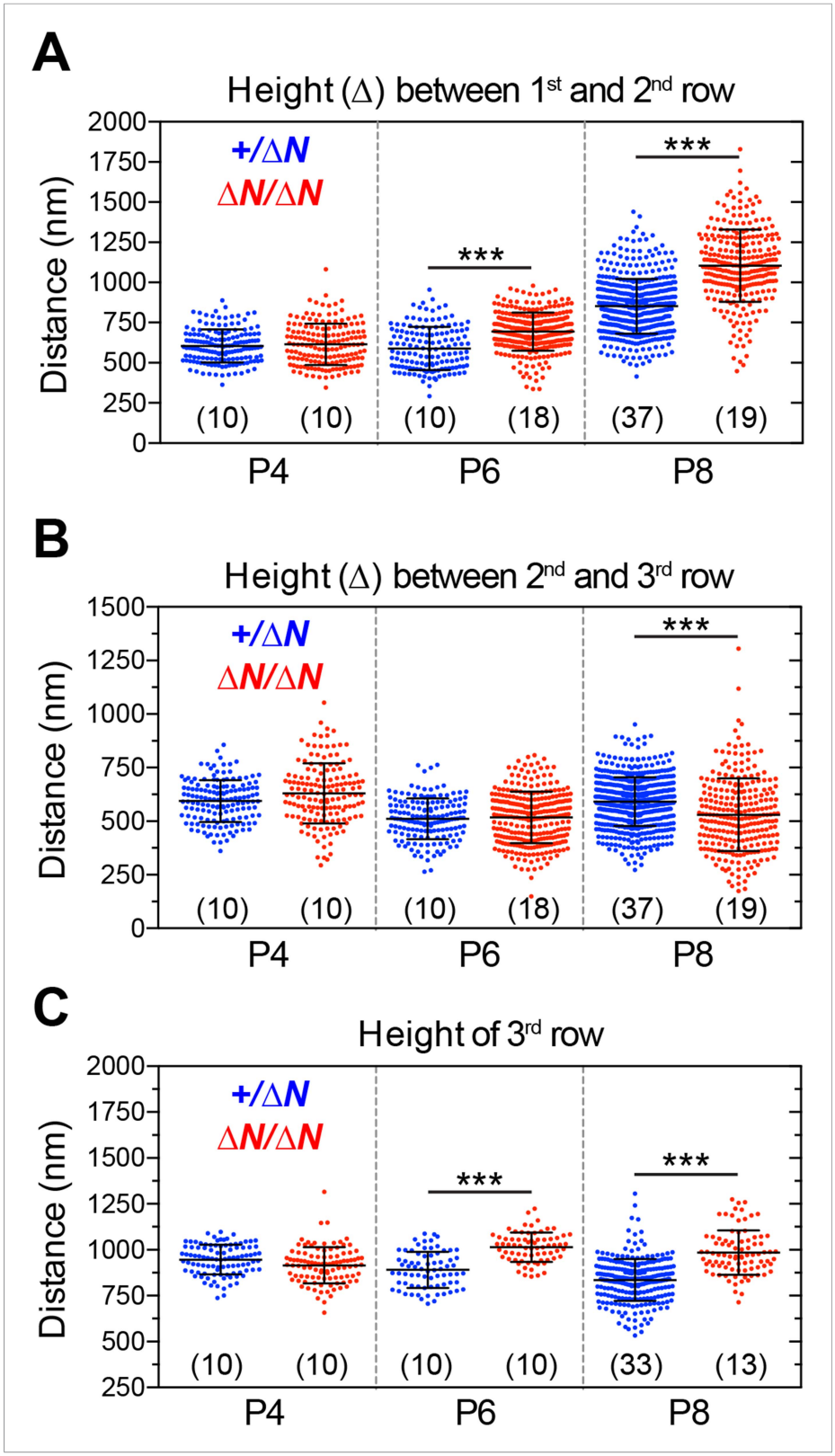

Figure 7—figure supplement 2. Analysis of stereocilia staircase architecture in *Myo15*$^{\Delta N/\Delta N}$ hair cells. (**A**–**C**) Tip to tip measurements of IHC stereocilia heights from SEM preparations of mutant *Myo15*$^{\Delta N/\Delta N}$ and normal hearing

Figure 7—figure supplement 2. continued on next page

Figure 7—figure supplement 2. Continued

Myo15$^{+/\Delta N}$ littermates at P4, P6 and P8. (**A**) Distance from the tip of the tallest stereocilia (first) row to the tip of the corresponding second row stereocilium. (**B**) Distance from the tip of the second stereocilia row to the third row. (**C**) Height of third row stereocilia. Each data point corresponds to an individual stereocilium with mean ± SD overlaid (number of hair cells sampled is shown in brackets). Asterisks indicate statistical significance: ***, $p < 0.0001$ (ANOVA with Tukey's multiple comparisons test). SEM images were obtained from cultured samples used for MET recordings (see also ***Figure 5***). The same images were analyzed in ***Figure 7—figure supplements 2, 3***.

DOI: 10.7554/eLife.08627.016

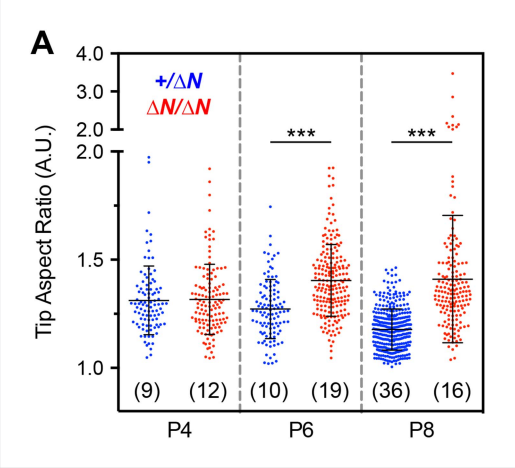

Figure 7—figure supplement 3. Analysis of stereocilia tip morphology in *Myo15*$^{\Delta N/\Delta N}$ hair cells. **(A)** Quantification of stereocilia tip shape from SEM preparations of mutant *Myo15*$^{\Delta N/\Delta N}$ and *Myo15*$^{+/\Delta N}$ IHCs at P4, P6 and P8. An ellipse was fitted to the tip of mechanotransducing stereocilia (second row) and used to calculate an aspect ratio (major axis divided by minor axis). An aspect ratio of 1 indicates a perfect circle, whilst aspect ratios >1 indicate elongation. Note the presence of aspect ratios >2 in mutant *Myo15*$^{\Delta N/\Delta N}$ hair cells at P8 (a split scale is used for the ordinate). Data points correspond to individual stereocilia with mean ± SD overlaid (number of hair cells sampled in brackets). Asterisks indicate statistical significance: ***, $p < 0.0001$ (ANOVA with Tukey's multiple comparisons test). SEM images were obtained from cultured samples used for MET recordings (see also ***Figure 5***). The same images were analyzed in ***Figure 7—figure supplements 2, 3***.

DOI: 10.7554/eLife.08627.017